Folding Type III Bricard Linkages

S. N. Lu * Beihang University, University of Genoa Beijing, P.R. China; Genoa, Italy

D. Zlatanov† University of Genoa Genoa, Italy

X. L. Ding‡ Beihang University Beijing, P.R. China

M. Zoppi§ University of Genoa Genoa, Italy

S. D. Guest¶ University of Cambridge Cambridge, UK

Abstract— *The paper presents a set of one-degree-of-freedom overconstrained linkages, which can be folded into a bundle and deployed into a polygon on a plane. The proposed mechanisms are movable Bricard octahedra of Type III, characterized by the existence of two configurations where all joints are coplanar. The possible geometries of doubly-collapsible Bricard linkages are parameterized and their kinematics is analyzed. A method is proposed to construct a bundle-compacting mechanism of this type, necessary and sufficient conditions are derived for the deployed-configuration polygon to be a square. Case studies and simulations validate the analysis and design.*

Keywords: type III Bricard linkage, bundle folding, deployable mechanism, overconstrained linkages

I. Introduction

A deployable mechanism (DM) is capable of configuration change which dramatically alters its shape and size. DMs have many potential applications, including for the rapid construction of structures both in space, e.g., antennas and telescopes [1–3], and on earth, in temporary and emergency architecture. A DM which is able to fold into a bundle is of particular interest: minimal size facilitates storage and transport. The most common DMs are composed of scissor-linkage elements, allowing, with good design, the mechanism to be folded into a bundle and deployed into different shapes [4, 5].

Recently, spatial overconstrained mechanisms have attracted the interest of designers of DMs. Pellegrino et al. studied a bundle-compacting Bennett linkage [6]. Similar research has also been done on the Myard linkage [7], and the Bricard linkages of types I (line-symmetric) and II (plane-symmetric) [6, 8–10]. The deployed shapes of the Bennett, and the Type I and II Bricard linkages, are a rhombus, a hexagon, and a rectangle, respectively.

Since it was proposed, the Type III Bricard linkage has attracted relatively less attention from researchers [11–14]. It has two collapsed configurations, i.e., all the six revolute joint axes (and the faces of the octahedron they define) collapse into a plane in two distinct ways. In this study, we discuss its parametrization and propose a method for the construction of a bundle-folding Type III Bricard linkage. In its other flat configuration, the mechanism deploys as a quadrangle or a hexagon.

The paper is organized as follows. In the following section, the type III Bricard linkage is reviewed and parameterized. Then, a geometric construction is described, demonstrating the existence of bundle-folding linkages of this type. Next, for a Bricard bundle with fixed length, the geometric conditions of forming the maximum deployed area are derived. Case studies have been performed on both forward and inverse design, and the obtained mechanisms have been simulated.

II. The Type III Bricard Linkage

Herein we analyze the type III Bricard linkages, which have two collapsible configurations. Due to the special geometric conditions each such mechanism must satisfy, it can be described by only five parameters.

A. Geometric construction

The Bricard linkage $ABCA'B'C'$ in Fig. 1, is of type III with two collapsed states. The linkage can be constructed as follows: draw two concentric circles of arbitrary radii; choose two arbitrary points A and A' outside of the larger circle; construct the tangents from A and A' to the circles and determine their intersections B, B', C and C'. The lines BC, $B'C'$, $B'C$ and BC' will be tangent to a third concentric circle with radius r_t. Then, the six triangles ABC', ABC, $AB'C$, $A'B'C$, $A'B'C'$, $A'BC'$ taken in this cyclic order and hinged at their common edges, constitute a deformable six-plate linkage with 1 dof [13].

*lvshengnan5@gmail.com
†zlatanov@dimec.unige.it
‡xlding@buaa.edu.cn
§zoppi@dimec.unige.it
¶sdg@eng.cam.ac.uk

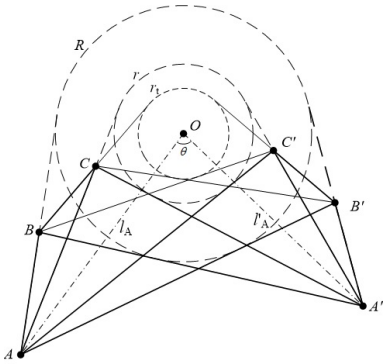

Fig. 1. Construction of a Bricard linkage

The six triangles in fact define a deformable octahedron: the two remaining (virtual) faces are the triangles ACB' and $A'C'B$, whose shape is constant during the movement. However, if they are physically part of the linkage, link interference is unavoidable.

B. Parametrization of the Bricard linkage

The construction in Fig. 1, can be described by the radii of the two circles and the positions of points A and A'. We denote the radii of the larger and smaller concentric circles by R and r, respectively. The lengths of OA and OA' are l_A and l'_A. The fifth parameter is the angle between OA and OA', denoted by θ. A linkage geometry of this type is described completely by the five scalars, R, r, l_A, l'_A, and θ. One of the parameters controls the scale of the Bricard linkage; the other four describe the collapsed configuration, which determines the shape and deformation of the octahedron.

C. The two coplanar configurations

The two collapsible configurations of an example Bricard linkage are shown in Fig. 2. The lighter color indicates the reverse side of the darker triangle.

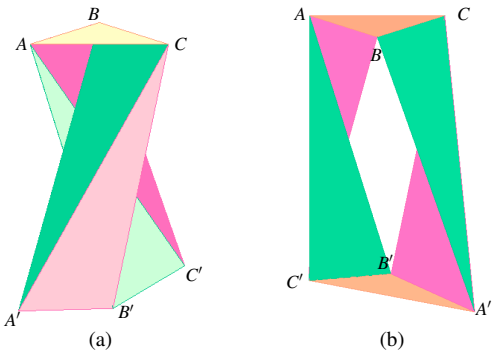

Fig. 2. Two collapsed configurations of the type III Bricard

III. Bundle-compacting Bricard Linkages

The geometric construction, described above, determines the relationship among the rotating axes which are the most important elements of the mechanism. The six triangles can be seen as connecting bars (physical links) with specific profiles. Kinetics of the linkage will not be affected by altering the geometric outline of the links, but the physical shape of the mechanism will change.

Consider the linkage made with the six triangles mentioned in the first paragraph of last section. The edges AB, BC, AC', $A'B'$, $B'C'$, $A'C$ are the rotation axes of the mechanism. In Fig. 2(a), draw a line not parallel to any of the six coplanar axes. Then, take the segment of this line connecting the intersection points on any two adjacent R-axes as the physical rigid link. Thus, in this shown configuration, the linkage will be compacted into a line (segment). Once the linkage moves to the other collapsible configuration, as shown in Fig. 2(b), a planar polygon will be formed by those connecting segments.

Practically, the rigid links have finite thickness and so in the first collapsed configuration, the physical shape of the mechanism will be a bundle; in the second, the top view of the mechanism forms a polygon.

Generally, it is desirable to minimize the distance between the extreme two intersection points on the bundle line, and to maximize the area of the polygon defined by the link segments in the other coplanar configuration. For this reason, one of the two collapsed states is preferred as the bundled configuration, and the other as the deployed one. As can be seen in Fig. 2, the hinge-axis segments (the common triangle edges) are more compactly located in Fig. 2(a) than in Fig. 2(b). Therefore, the length of the segment on the bundle line will be shorter in Fig 2(a).

Different choices of the intersecting line in Fig. 2(a), result in different deployed shapes and sizes in the second coplanar configuration. Figure 3 gives three examples. The Bricard linkage in Fig. 3 satisfies $AB = BC = A'B' = B'C'$.

The bundle line intersects either a hinge-axis segment or its extension. In Fig. 3(a), the straight line crosses AB, AC', $A'B'$, $A'C$ and the extensions of BC and $B'C'$, in addition, it is parallel with BB'. The formed geometric shape in the other coplanar configuration is a hexagon which has three pairs of parallel sides.

The straight line in Fig. 3(b) is BB', intersecting two axes (AB and BC) at B, and two others ($A'B'$ and $B'C'$) at B'. There are only four intersection points of the line with the six axes.Therefore, in the coplanar configuration on the right, the formed shape is a quadrangle.

In Fig. 3(c), the straight line crosses BC, AC', $A'C$, $A'B'$, and the continuations of AB and $B'C'$. The formed shape is a hexagon, however, the shape is more general than in Fig. 3(a).

Among all the possible lines, BB' is the shortest segment that can cross all six rotation axes. A simulated model of

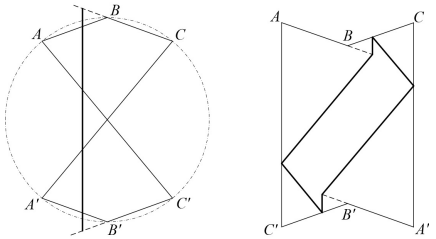

Fig. 3. Bundle-folding linkages form different deployed polygons

this case is shown below.

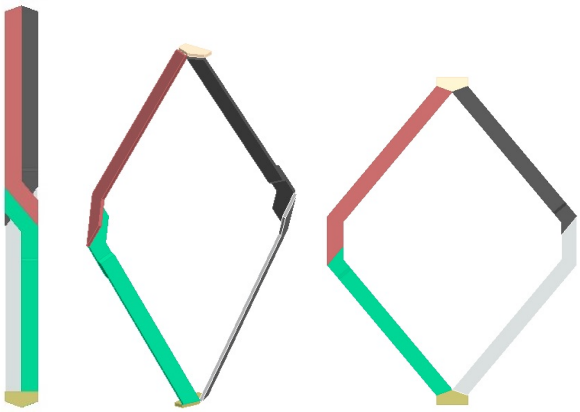

Fig. 4. Simulation of a bundle-folding Bricard square

In Fig. 4, the bundle line forms a quadrangle in the other collapsible configuration. In the simulated model, as the links must have some physical shape and non-zero-area cross-sections, the outline of the mechanism varies a little. In the following analysis, we will only focus on the shape formed by the line, since the link-shape can vary depending on the detailed practical realization.

IV. The maximum deployed area of the folded bundle

When the intersecting line is along BB', the deployed area will be a quadrangle. In this section, the conditions of obtaining a linkage that yields a maximum deployed area are analyzed. Inverse analysis is also performed, obtaining all the parameter sets yielding a bundle-folding Bricard mechanism with a given bundle length.

It is well-known that among the quadrangles with the same perimeter, the square has the maximum area. Therefore, we seek the conditions under which the Bricard linkage will deploy into a square.

A. *Deployable square*

A general type III Bricard linkage is shown in Fig. 5. The bundle line is BB'. The common point of BB' and $A'C$ is D, while BB' and AC' intersect at D'. The six rotation axes are AB, BC, $A'C$, $A'B'$, $B'C'$, and AC'. As the linkage moves, the distance between B and B' (which are not on the same face of the octahedron) changes, while points D and D' stay on the rigid intervals $A'C$ and AC', respectively. The deployed quadrangle has its vertices at the positions of B, D, B' and D' in the alternative collapsed configuration.

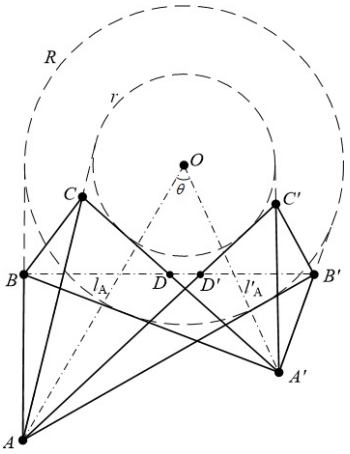

Fig. 5. Construction of Bricard linkage

Figure 6 illustrates a general bundle-folding Bricard quadrangle. The two collapsed configurations are displayed in Fig. 6: $ABCA'B'C'$ and $ABC_*A'_*B'_*C'$, respectively. Triangle ABC' is assumed to be the fixed base link. An asterisk denotes the position of a moving point in the second coplanar configuration. The octahedron vertices B' and C rotate about AC' and AB, respectively. Therefore, B' and B'_* are symmetric with respect to AC', i.e., $|B'D'| = |B'_*D'|$. Similarly, $|BD| = |BD_*|$. The distance between points on the same rigid link does not change. Hence, $|B'D| = |B'_*D_*|$, as a segment on the rigid panel $A'B'C$. So, with known length

of BB' and location of D and D', the lengths of the four sides of the quadrangle $BD'B'_*D_*$ can be obtained.

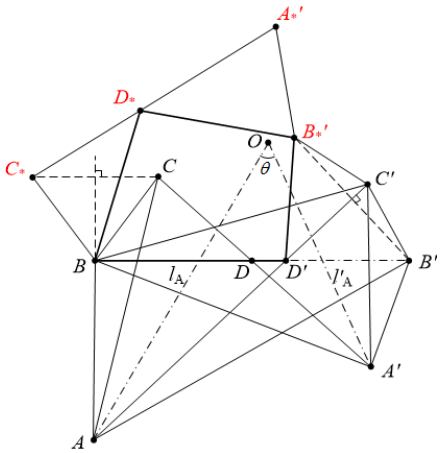

Fig. 6. The formed quadrangle

A.1 Geometric conditions

The Bricard linkage in Fig. 6 must satisfy the following three geometric conditions for the quadrangle $BD'B'_*D_*$ to be a square.

(i) AC', $A'C$ and BB' have a common point, $D = D'$
(ii) This intersection is at the midpoint of BB'
(iii) $\angle C'DB' = 45°$

(i) $D = D' \Leftrightarrow |BD'| = |BD_*|$ & $|B'_*D'| = |B'_*D_*|$

Proof
Sufficiency. Because $B'D$ belongs to the rigid body $A'B'C$, $|B'D| = |B'_*D_*|$. Similarly $|B'D'| = |B'_*D'|$, since $B'D'$ stays on another rigid panel, $AB'C'$. If $D = D'$, then $|B'D| = |B'D'|$. Therefore, $|B'_*D_*| = |B'_*D'|$, i.e., the two sides of the quadrangle at B'_* are equal. As $|BD_*| = |BD|$, when $D = D'$, $|BD_*| = |BD'|$, i.e., the quadrangle has a kite shape.
Necessity. Obvious: $|BD'| = |BD_*|$ is equivalent to $|BD| = |BD'|$, so D coincidences with D'. □

Once condition (i) is met, there exists one symmetry axis, BB'_1, of the deployed quadrangle. Moreover, $OD \perp BB'$, Fig. 7.

(ii) $D = D'$ is the midpoint of $BB' \Leftrightarrow BD'B'_*D_*$ is a rhombus

Proof
Sufficiency. When, in addition to Condition (i), $D = D'$ is the midpoint of BB', $|BD| = |B'D|$, and so $|BD| = |B'_*D|$. The four sides of the quadrangle are equal and $BD'B'_*D_*$ is a rhombus.
Necessity. If $BD'B'_*D_*$ is a rhombus, then its four sides are equal, and so are $|BD|$ and $|B'D|$. Therefore, D and D' coincide and divide BB' in two equal segments. □

By adding constraint (ii), a second mirror-symmetry axis is defined, Fig. 8.

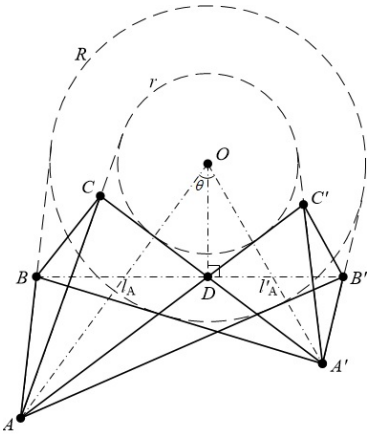

Fig. 7. AC', $A'C$ and BB' intersect at a same point

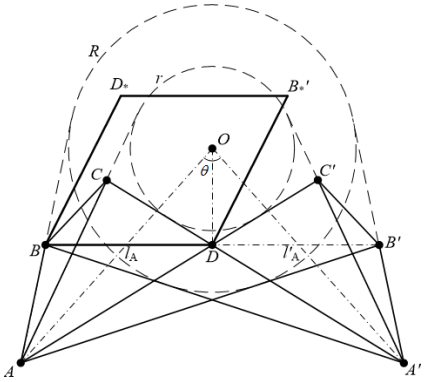

Fig. 8. The formed rhombus

(iii) $\angle C'DB' = 45° \Leftrightarrow BD'B'_*D_*$ is a square

Proof
Sufficiency. Since the rigid panel $AB'C'$ rotates around axis AC' in Fig. 8, $\angle B'DB'_* = 2\angle C'DB'$ in the other coplanar configuration, and $\angle BDB'_* = 180° - \angle B'DB'_*$. When $\angle C'DB' = 45°$, $\angle B'DB'_*$ is a right angle. $BD'B'_*D_*$ is a square as it is a rhombus that includes a right angle (see Fig. 9).
Necessity. Obvious. □

A.2 Dependence of the geometric parameters

With the above three geometric conditions satisfied, only two of the five Bricard-geometry parameters are independent. In the following, the relationships among the five geometric parameters of the Bricard linkage are derived.

First, conditions (i) and (ii) are assumed. We show that then there are three independent parameters determining the mechanism geometry.

When $D = D'$ and $|BD| = |DB'|$, points B and B' are symmetric with respect to OD, Fig. 8. Due to $OD \perp BB'$, we have $|OB| = \sqrt{|OD|^2 + |BD|^2} = |OB'| = \sqrt{|OD|^2 + |B'D|^2}$. It can be concluded, from the construction of the type III Bricard linkage, that A and A' are located on the intersec-

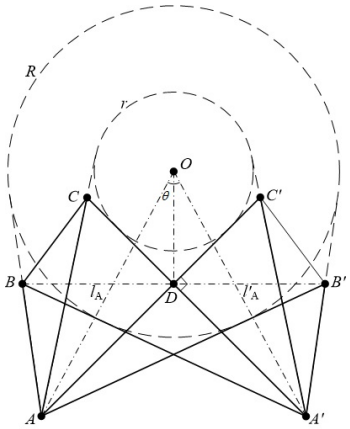

Fig. 9. The formed square

tion of the tangent lines from B and B', which are also symmetric with respect to OD. In Fig. 10, there are two pairs of points of tangency: P_1, P_2 and P_1', P_2', on the tangents from B and B', respectively.

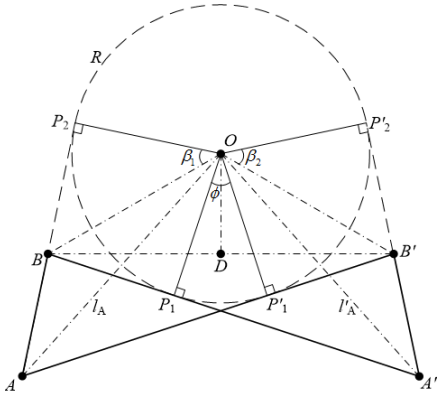

Fig. 10. D locates in the middle of BB'

The angles $\angle P_2OB$ and $\angle P_2'OB'$ are, respectively,

$$\cos\beta_1 = \frac{R}{|OB|} \tag{1}$$

$$\cos\beta_2 = \frac{R}{|OB'|} \tag{2}$$

where $\beta_1, \beta_2 \in [0, 180^\circ]$. Because $|BD| = |B'D|$, we have $\beta_1 = \beta_2$.

If $\angle P_1OP_1' = \phi$, then $\angle P_2OP_1' = 2\beta_1 + \phi$ and $\angle P_2'OP_1 = 2\beta_2 + \phi$, which gives

$$\angle P_2OA = \angle P_2'OA' = \frac{2\beta_1 + \phi}{2} = \delta \tag{3}$$

Since $R = l_A\cos\delta = l_A'\cos\delta$,

$$l_A = l_A' \tag{4}$$

In the following, we derive R as a function of l_A, θ and r.

From $l_A = l_A'$ we have $\angle OAB' = \angle OA'B'$. So,

$$\kappa_1 + \kappa_2 = \kappa_1 + \angle OAB' + \kappa_2 - \angle OA'B' = \angle OAA' + \angle OA'A. \tag{5}$$

where $\kappa_1 = \angle B'AA'$ and $\kappa_2 = \angle B'A'A$. Therefore, $\kappa = \pi - \kappa_1 - \kappa_2 = \theta$, which means that points O, A, A', B' are on the same circle, and so is B.

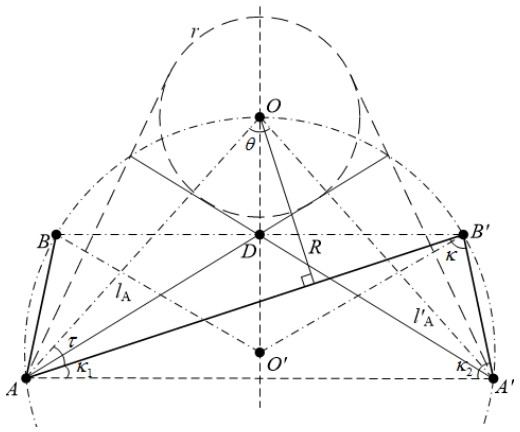

Fig. 11. Relationship among l_A, θ and r

Because A and A' are symmetric with respect to the line OD, the latter must pass through the center, O' of this circle. For its diameter, we have

$$d = \frac{l_A}{\cos\dfrac{\theta}{2}} \tag{6}$$

From the circle with radius r,

$$|OD| = \frac{r}{\sin(\dfrac{\theta}{2} + \arcsin\dfrac{r}{l_A})} \tag{7}$$

we have

$$|O'D| = \frac{1}{2}d - |OD| \tag{8}$$

and

$$\angle DO'B = \arccos\frac{|O'D|}{\frac{1}{2}d} = \arccos(1 - \frac{2r\cos\dfrac{\theta}{2}}{\sin\dfrac{\theta}{2}\sqrt{l_A^2 - r^2} + \cos\dfrac{\theta}{2}r}) \tag{9}$$

Because all the points are located on a circle, the central angle $\angle BO'B'$ is 2 times of the angle of circumference $\angle OAB'$. So

$$\tau = \angle OAB' = \frac{1}{2}\arccos(1 - \frac{2r\cos\dfrac{\theta}{2}}{\sin\dfrac{\theta}{2}\sqrt{l_A^2 - r^2} + \cos\dfrac{\theta}{2}r}) \tag{10}$$

Since the circle with radius R is tangent to AB',

$$R = l_A \sin\tau \tag{11}$$

In the second step, all the three conditions from the previous subsection constrain the mechanism. So, B'_* will locate on OD and θ becomes a function of l_A and r,

$$\theta = 90^\circ - 2\arcsin\frac{r}{l_A} \tag{12}$$

B. Bricard linkages with the same bundle length

In the following, we obtain a Bricard linkage that can be deployed into a square for a given length of the bundle.

From the above calculations, the deployed square can be determined by two parameters, e.g., r and l_A in (12). There are infinitely many linkages that can be deployed into a square and fold into a bundle with same length. By varying the above equations, the relationship among r, l_A and BB' is obtained,

$$\frac{4\sqrt{2}rl_A}{\cos(45^\circ - \arcsin\frac{r}{l_A})} - 8r^2 = |BB'|^2 \tag{13}$$

Therefore, with given BB' and r, l_A can be calculated with (13). The other parameters can be obtained from (12), (11), and (4).

V. Case studies

Two case studies are reported in this section. The first outlines a procedure to obtain a Bricard linkage deployable into a square shape. The second describes several different Bricard linkages with the same bundle length but different geometric parameters.

A. Case I

In this case study, we start from a general Bricard linkage, then constrain the deployed shape to a square by adding the constraints step by step.

We take the Bricard linkage in Fig. 5 as the model. The 5 parameters of the initial mechanism are $R = 35$, $r = 20$, $l_A = 70$, $l'_A = 50$, $\theta = 55^\circ$. The bundle line is BB' as usual, the deployed shape is in Fig. 6.

From (4) and (11), adding the first two constraints, we have

$$l_A = l'_A = 50 \tag{14}$$

$$R = 33.77 \tag{15}$$

The bundle and the corresponding deployed rhombus is shown in Fig. 12. When $\theta = 90^\circ - 2\arctan\frac{r}{l_A} = 42.84^\circ$, the obtained shape is a square as described in Fig. 13.

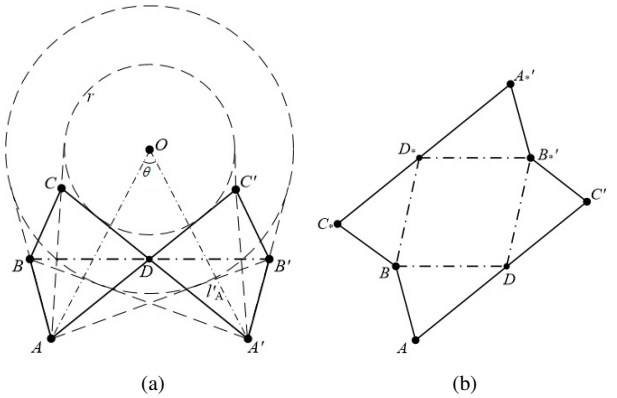

Fig. 12. A Bricard linkage unfolding into a rhombus

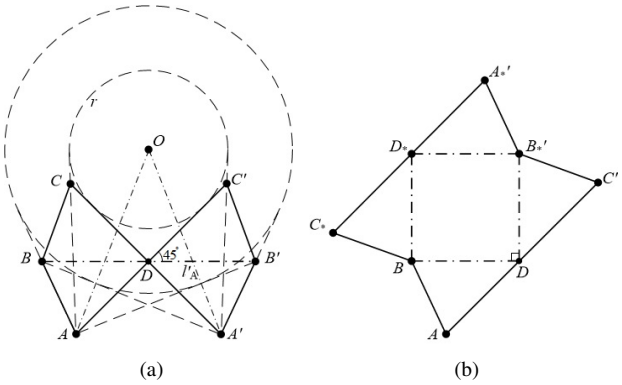

Fig. 13. A Bricard linkage unfolding into a square

B. Case II

With the same given length $|BB'| = 200$ and different values r, several Bricard linkages are obtained, each of them deployable into a square.

When $r = 110$, from (13), the other parameters are calculated as $l_A = l'_A = 213.35$, $\theta = 27.93^\circ$, $R = 179.47$. The construction of the Bricard linkage and the formed square is shown in Fig. 14.

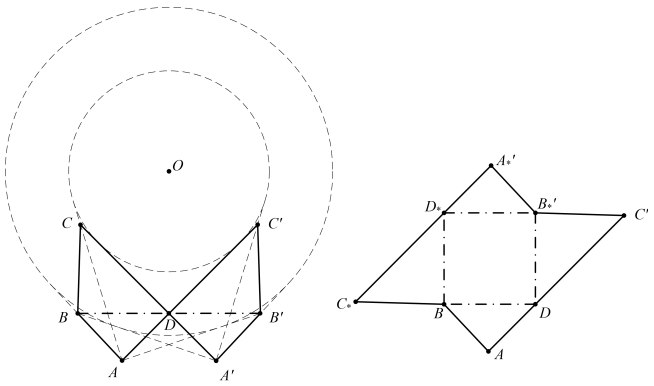

Fig. 14. Construction of the Bricard linkage with $BB' = 200$ and $r = 110$

Next, we use $r = 70.71$, $l_A = 184.78$, $\theta = 45^\circ$, and $R =$

130.66. This is a special case, since D and D_* are midpoints of AC' and A'_*C_* respectively, Fig. 15.

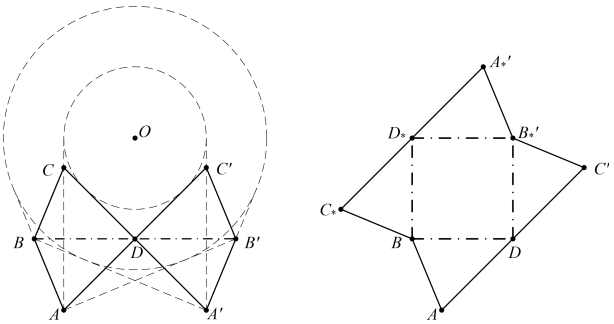

Fig. 15. Construction of the Bricard linkage with $BB' = 200$ and $r = 70.71$

When $r = 45$, $l_A = 188.82$, $\theta = 62.42$, and $R = 97.87$, the two collapsed configurations are shown in Fig. 16.

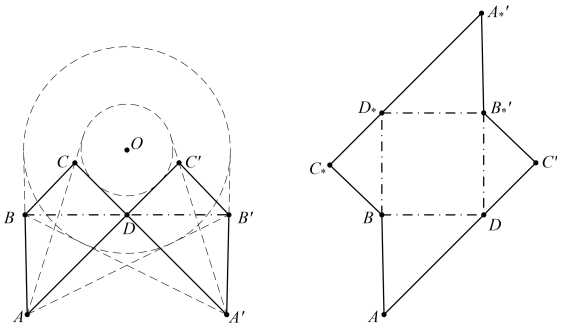

Fig. 16. Construction of the Bricard linkage with $BB' = 200$ and $r = 45$

It can be seen that, under the condition that the bundle length is constant, the smaller the value of r, the nearer point D_* is to C_*. When $r = \frac{\sqrt{2}}{4}|BB'|$, D is in the midpoint of $A'C$ and AC'.

A 3D model of the Bricard linkage in Fig. 14 has been built where the cross section of each bar is nearly a rectangle, but slightly modified to avoid collisions during the motion. Simulation of the movement of the bundle-folding Bricard linkage is performed as shown in Fig. 17. The formed square is marked with a dotted line in Fig. 17(c).

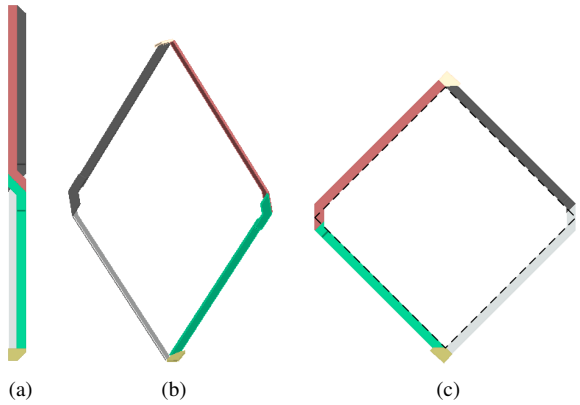

Fig. 17. Simulation of an example Bricard linkage

VI. Conclusion

Using the capability of the type III Bricard linkage to be coplanar in two configurations, a family of mechanisms has been proposed, each of which can be folded into a bundle and deployed into a planar polygon. The functional relationships among the bundle length, the deployed shape, and the parameters of the Bricard linkage have been analyzed, and the geometric conditions for the construction of a deployable square have been derived.

Case studies have been performed, presenting the procedure of obtaining a deployed square, with several choices of the Bricard linkage with the same bundle length and deployed shape.

Although the paper focuses on the construction of deployable quadrangles, with a different choice of the bundle line the mechanism can be also deployed as a hexagon.

Acknowledgement

This research has been supported by the AUTORECON project funded under the Seventh Framework Program of the European Commission (Collaborative Project NMP-FOF-2011-285189), National Natural Science Funds (of China) for Distinguished Young Scholar under Grant 51125020, and the National Natural Science Foundation of China under Grant 51275015. The authors gratefully acknowledge the supporting agencies.

References

[1] F. Escrig, J. P. Valcarcel, and J. Sanchez. Deployable cover on a swimming pool in Seville. *Bulletin of the International Association for Shell and Spatial Structures*, 37(1):39–70, 1996.

[2] J. S. Zhao, J. Y. Wang, F. L. Chu, et al. Mechanism synthesis of a foldable stair. *Journal of Mechanisms and Robotics*, 4(1):014502, 2012.

[3] G. Durand, M. Sauvage, A. Bonnet, et al. Talc: a new deployable concept for a 20-m far-infrared space telescope. In *SPIE Astronomical Telescopes+ Instrumentation*, pages 91431A–91431A. International Society for Optics and Photonics, 2014.

[4] F. Maden, K. Korkmaz, and Y. Akgün. A review of planar scissor structural mechanisms: geometric principles and design methods. *Architectural Science Review*, 54(3):246–257, 2011.

[5] J. S. Zhao, F. L. Chu, and Z. J. Feng. The mechanism theory and application of deployable structures based on SLE. *Mechanism and Machine Theory*, 44(2):324–335, 2009.
[6] S. Pellegrino, C. Green, S. D. Guest, et al. *SAR advanced deployable structure*. University of Cambridge, Department of Engineering, 2000.
[7] X. Z. Qi, Z. Q. Deng, B. Li, et al. Design and optimization of large deployable mechanism constructed by Myard linkages. *CEAS Space Journal*, 5(3-4):147–155, 2013.
[8] Y. Chen, Z. You, and T. Tarnai. Threefold-symmetric Bricard linkages for deployable structures. *International journal of solids and structures*, 42(8):2287–2301, 2005.
[9] J. Cui, H. L. Huang, B. Li, et al. A novel surface deployable antenna structure based on special form of Bricard linkages. In *Advances in Reconfigurable Mechanisms and Robots I*, pages 783–792. Springer, 2012.
[10] A. D. Viquerat, T. Hutt, and S. D. Guest. A plane symmetric 6R foldable ring. *Mechanism and Machine Theory*, 63:73–88, 2013.
[11] R. Bricard. Mémoire sur la théorie de l'octaèdre articulé. *Journal de Mathématiques pures et appliquées*, pages 113–148, 1897.
[12] A. V. Bushmelev and I. K. Sabitov. Configuration spaces of Bricard octahedra. *Journal of Mathematical Sciences*, 53(5):487–491, 1991.
[13] M. Goldberg. Linkages polyhedral. *National Mathematics Magazine*, 16(7):323–332, 1942.
[14] J. E. Baker. On the skew network corresponding to Bricard's doubly collapsible octahedron. *Proceedings of the Institution of Mechanical Engineers, Part C: Journal of Mechanical Engineering Science*, 223(5):1213–1221, 2009.